CENTENNIAL FEATURE ARTICLE

Photodynamics in Complex Environments: *Ab Initio* Multiple Spawning Quantum Mechanical/Molecular Mechanical Dynamics[†]

Aaron M. Virshup,[‡] **Chutintorn Punwong,**[§] **Taras V. Pogorelov,**[||] **Beth A. Lindquist,**[||] **Chaehyuk Ko,**[||] **and Todd J. Martínez**[*,§,||]

Center for Biophysics and Computational Biology, Department of Chemistry, and Department of Physics, University of Illinois, Urbana, Illinois, 61801

Received: August 16, 2008; Revised Manuscript Received: October 8, 2008

Our picture of reactions on electronically excited states has evolved considerably in recent years, due to advances in our understanding of points of degeneracy between different electronic states, termed "conical intersections" (CIs). CIs serve as funnels for population transfer between different electronic states, and play a central role in ultrafast photochemistry. Because most practical photochemistry occurs in solution and protein environments, it is important to understand the role complex environments play in directing excited-state dynamics generally, as well as specific environmental effects on CI geometries and energies. In order to model such effects, we employ the full multiple spawning (FMS) method for multistate quantum dynamics, together with hybrid quantum mechanical/molecular mechanical (QM/MM) potential energy surfaces using both semiempirical and *ab initio* QM methods. In this article, we present an overview of these methods, and a comparison of the excited-state dynamics of several biological chromophores in solvent and protein environments. Aqueous solvation increases the rate of quenching to the ground state for both the photoactive yellow protein (PYP) and green fluorescent protein (GFP) chromophores, apparently by energetic stabilization of their respective CIs. In contrast, solvation in methanol retards the quenching process of the retinal protonated Schiff base (RPSB), the rhodopsin chromophore. Protein environments serve to direct the excited-state dynamics, leading to higher quantum yields and enhanced reaction selectivity.

Introduction

As demonstrated by numerous ultrafast spectroscopic experiments,[1] reactions on electronically excited states are some of the fastest chemical reactions known. Our understanding of the mechanisms of these reactions has evolved considerably in past years, largely due to the recognition that potential energy surfaces corresponding to different electronic states may become exactly degenerate at specific molecular geometries, and that such points of degeneracy are both frequent and energetically accessible. These degeneracy points are known as conical intersections[2−5] because they have the shape of a double cone; i.e., the electronic degeneracy is lifted in first order by geometric displacements about the intersection geometry. Most of the possible displacements do not lift the degeneracy, so these points are better thought of as "seams" embedded in the $(3N−6)$-dimensional space of all possible molecular displacements. The displacements that do lift the degeneracy are collectively called

the "branching space", and there are precisely two such displacements for most conical intersections involving two electronic states. However, it is also possible for three (or even more) electronic states to be simultaneously degenerate at a given molecular geometry, and the dimension of the branching space increases in these cases. It is rapidly becoming apparent that such three-state intersections are far from rare,[6,7] and may play a key role in the photochemistry of many molecules such as the DNA bases[8] and excited-state intramolecular proton transfer processes.[9,10]

Conical intersection geometries serve as gateways to lower (or in some cases, higher[11]) electronic states due to the complete breakdown of the Born−Oppenheimer approximation in their vicinity. Because of their central role in photochemistry, a number of algorithms have been developed to locate conical intersection geometries, in much the same way that one would locate local minima and transition states for reactions occurring entirely on a single (usually the ground) electronic state. Because conical intersection geometries form a high-dimensional seam, it is not enough to locate *any* such geometry and it has become common to characterize CIs by the lowest energy point on the seam.[12,13] These minimal energy conical intersections (MECIs) may or may not always be relevant to the dynamical processes of interest. Often, MECIs lie considerably below the Franck−Condon point and the molecule may be far from equilibrium when it reaches an intersection. Thus, it is often the case that initial conditions and kinetic energy matter tremendously and the

‡ Department of Physics.
§ Center for Biophysics and Computational Biology.
|| Department of Chemistry.

Centennial Feature Article

J. Phys. Chem. B, Vol. 113, No. 11, 2009 **3281**
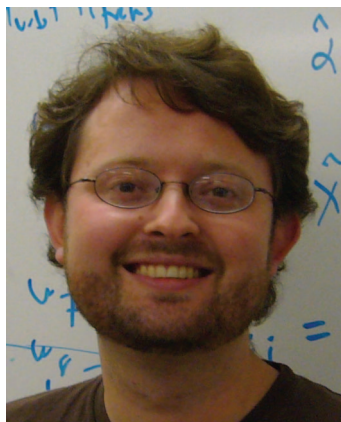
Aaron M. Virshup received a B.A. in Physics from Grinnell College in 2003 and an M.A. in Physics from UIUC in 2004. His research interests include development and application of QM/MM techniques for ultrafast photodynamics and coarse-grained analyses of reaction dynamics.

Beth Lindquist was born in Columbus, Ohio, in 1985. She received her B.S. in Biochemistry from the University of Notre Dame in 2007. Currently, she is a graduate student working with Prof. Todd Martínez at UIUC. Her research focuses on theoretical studies of the photodynamics of the GFP chromophore.

Chutintorn Punwong was born in Thailand. She received her B.Sc. in Physics from Prince of Songkla University, Songkla, Thailand, in 2002. She is currently a graduate student in the Biophysics program at UIUC working under the supervision of Prof. Todd Martínez. Her research focuses on modeling the photodynamics of retinal protonated Schiff base (RPSB) in different environments to understand the influences of these surroundings on the selectivity and efficiency of photoisomerization of RPSB in the rhodopsin protein family.

Chaehyuk Ko received a B.S. in Chemistry in 2001 from Seoul National University and a Ph.D. in Chemistry in 2008 from UIUC. His current research interests include the photodynamics of the photoactive yellow protein chromophore and efficient electronic structure methods for optical excitations in large molecular systems.

Taras V. Pogorelov is a postdoctoral research associate at UIUC working with Todd J. Martínez. His previous degrees include a Diploma in biomedical engineering from Bauman Moscow State Technical University and a M.S. in mathematics from UIUC. He received his Ph.D. in Chemical Physics in 2006 from UIUC while working on the development and application of molecular dynamics methods for protein folding and protein−protein interaction. His current interests include application and development of multiple spawning QM/MM methodology with a concentration in the photochemistry of GFP and its variants.

Todd J. Martínez received his B.S. in Chemistry from Calvin College (1989) and his Ph.D. in Chemistry from UCLA (1994). After spending two years as a Fulbright Postdoctoral Researcher at the Hebrew University in Israel, he joined the faculty at UIUC, where he currently holds a Gutgsell Chair in Chemistry. His research is focused on the study of electronic structure and chemical dynamics in excited electronic states.

portions of the intersection seam where population transfer occurs may be far removed (energetically and/or geometrically) from the nearest MECI. There have been a number of attempts

to map out the structure of intersection spaces in order to better understand excited-state reactivity.[14-17] These approaches can be quite useful, but a more direct approach is to follow the dynamics of the molecule and subsequently reduce the dynamics to a mechanism. There has been considerable recent progress on this front, with new dynamical methods capable of going beyond the Born−Oppenheimer approximation coupled to first principles calculations of the intermolecular forces by solving the electronic Schrödinger equation during the dynamics.[18-25] This *ab initio* molecular dynamics strategy has the distinct advantage of allowing arbitrary bond rearrangement, avoiding complicated multidimensional fitting of potential surfaces and their couplings, and eschewing preconceptions about the character of the relevant electronic states.

Most practical photochemistry occurs in solution, and considerable current interest in excited-state reactivity stems from its role in both natural and artificial molecular machines, such as biological photoreceptors[26] and light-triggered or light-powered molecular devices.[27-29] Thus, it is important to understand the role of complex environments in shaping and directing photochemistry. It can be expected that both electrostatic and steric effects will alter the geometries and energies of conical intersections, and that these effects will have both static and dynamic character. For example, it has been shown that conical intersections can be stabilized in solvent in some cases[30] and that they can disappear completely in other cases.[31] Completely first principles simulation of excited-state dynamics in complex environments is currently a major unmet challenge to theoretical and computational chemistry. Several intermediate approaches have been pursued, ranging from fully atomistic hybrid quantum mechanical/molecular mechanical (QM/MM) methods[32-34] to mean-field[35,36] and polarizable dielectric[31,37] methods. In this article, we focus on the role of solvent and protein environments in photochemical reactions of several chromophores that undergo photoinduced *cis−trans* isomerization. We present a brief overview of the methods used, and for each of the chromophores, we compare the excited-state dynamics in different environments.

Theory

***Ab Initio* Multiple Spawning Quantum Dynamics.** The full multiple spawning (FMS) method for quantum molecular dynamics uses a classically motivated set of nuclear basis functions in order to describe the quantum mechanical time evolution of a system including transitions between electronic states. This method has been extensively described elsewhere,[19,38] and we present only a brief overview here. The FMS wave function ansatz is a linear combination of time-dependent Born−Oppenheimer basis functions:

$$\Psi_{\text{FMS}}(\mathbf{R}, \mathbf{r}, t) = \sum_{I=1}^{N(t)} c_I(t)\, \chi_I(\mathbf{R}, t)\, \phi_{N_I}(\mathbf{r};\mathbf{R}) \qquad (1)$$

where $\chi_I(\mathbf{R},t)$ is a nuclear basis function and ϕ_{N_I} is the electronic wave function on state N_I. The nuclear basis functions are minimum uncertainty Gaussian wavepackets[39] in each of the nuclear coordinates, and their average positions and momenta are chosen to evolve classically on the potential energy surface (PES) for the electronic state with which they are associated. The widths of the Gaussian basis functions are chosen to be isotropic and time-independent. The precise width for each atom is chosen to achieve maximum overlap with the ground vibrational wave function in the harmonic approximation for a

test set of organic molecules, subject to the constraint that the widths are isotropic and depend only on the atomic mass. The time evolution of the complex amplitudes $c_I(t)$ is determined by direct substitution of the wave function ansatz in eq 1 into the time-dependent Schrödinger equation.

When a nuclear wavepacket associated with a given electronic state enters a region of high nonadiabatic coupling to a different electronic state, the number of basis functions $N(t)$ is expanded, and a new basis function is placed on the complementary PES (initially with zero amplitude). This dynamic "spawning" of new basis functions allows description of population transfer between different PESs without any prior knowledge of their characteristics. The FMS dynamics method uses only local information about the PESs and their nonadiabatic couplings, so it is ideally suited to implementation in an *ab initio* molecular dynamics context, i.e., where the PESs and their couplings are evaluated "on the fly" by solving the electronic structure problem during the dynamics. This combination of FMS and *ab initio* molecular dynamics is referred to as *ab initio* multiple spawning (AIMS), and is the method used for the work described here. All dynamical simulations were performed in our implementation of AIMS using the MOLPRO[40] or MOPAC[41] electronic structure packages, and details have been given previously.[42]

QM/MM Potential Energy Surfaces. Modeling of excited-state dynamics in complex environments within a fully *ab initio* approach is currently too computationally demanding. Fortunately, in many cases, it is not necessary, since the electronic excitation is often localized on a well-defined chromophore. Thus, hybrid quantum mechanical/molecular mechanical (QM/MM) methods, as pioneered by Warshel[43] and further developed by many others,[44-47] are particularly appropriate. In QM/MM schemes, the system is partitioned into two regions. The "QM" region, usually the smaller one, is modeled with *ab initio* (or possibly semiempirical) quantum mechanical techniques and represents a chemically active region where bond rearrangement and/or electronic excitation can be described. The "MM" region, generally corresponding to the environment surrounding the QM system, is modeled with a molecular mechanical force field. This partitioning gives rise to the approximate electronic Hamiltonian

$$\hat{H}_{\text{el}} \cong \hat{H}_{\text{QM}} + \hat{H}_{\text{MM}} + \hat{H}_{\text{QM/MM}} \qquad (2)$$

where $\hat{H}_{\text{QM}}$ is the exact Hamiltonian for the QM system, $\hat{H}_{\text{MM}}$ the force field of the MM system, and $\hat{H}_{\text{QM/MM}}$ the interaction between the two systems.

The interaction between the two systems is separated into three components: Lennard-Jones, electrostatic, and bonding:

$$\hat{H}_{\text{QM/MM}} = \hat{H}_{\text{LJ}} + \hat{H}_{\text{ES}} + \hat{H}_{\text{bond}} \qquad (3)$$

The intersystem Lennard-Jones interaction

$$\hat{H}_{\text{LJ}} = \sum_{\substack{i \in \text{MM atoms} \\ j \in \text{QM atoms}}} 4\varepsilon_{ij}\left[\frac{\sigma_{ij}}{R_{ij}^{12}} - \frac{\sigma_{ij}}{R_{ij}^{6}}\right] \qquad (4)$$

represents dispersion and Pauli repulsion between entire atoms in the QM and MM regions. The terms ε_{ij} and σ_{ij} are empirical parameters drawn from the MM force field, and R_{ij} is the interatomic separation. As usually implemented, this term does

Centennial Feature Article

J. Phys. Chem. B, Vol. 113, No. 11, 2009 **3283**

not include electronic coordinates, and thus neglects coupling of the QM electronic wave function to the MM system via these forces.

The electrostatic interaction term, in contrast, *does* include electronic coordinates, and thus must be included in the electronic structure calculation. This interaction is given by

$$\hat{H}_{ES} = \sum_{\substack{i \in \text{MM atoms} \\ j \in \text{QM nuclei}}} \frac{q_i Q_j}{R_{ij}} + \sum_{\substack{i \in \text{MM atoms} \\ j \in \text{QM electrons}}} \frac{-q_i}{|\mathbf{R}_i - \hat{\mathbf{r}}_j|} \quad (5)$$

where the first sum represents electrostatic interactions between MM atoms and QM nuclei, while the second represents interaction between the electrons in the QM system and the point charges in the MM system. The second sum, in particular, couples the electronic structure of the QM system to the MM system.

In QM/MM simulations of the chromophores in protein environments, the QM and MM regions can be connected through covalent bonds via connection atoms, represented by the bonding term $\hat{H}_{bond}$. In our semiempirical calculations, the connection atoms are treated the same way as the QM part but with a special set of parameters.[48,49] For *ab initio* QM/MM methods, we have previously discussed the use of a multicentered valence electron effective potential (MC-VEEP) approach,[50] which ensures the correct behavior of the link atom for ground and excited states. For all results presented here, MM force field parameters were drawn from the Amber94 force field[51–53] with the rigid TIP3P model for water[54] and OPLS/AA parameters for methanol.[55]

***Ab Initio* Electronic Structure.** The choice of QM method is an important factor in both the cost and accuracy of a given QM/MM calculation. Multireference *ab initio* techniques are uniquely well suited for the description of excited-state chemistry because they can describe bond rearrangement and near-degeneracy around conical intersections correctly, and in principle require no system-dependent tuning. In practice, only a limited set of references can be included and it is therefore very important to calibrate the chosen method. We do this by verifying that the ordering of electronic states and relative energies of important points such as excited-state minima and MECIs are consistent with more accurate techniques that are too computationally demanding for use in dynamics calculations.[56] This process is typically iterative, with initial dynamics calculations being used to identify important minima and/or MECIs, that are then used for verification and validation by more accurate electronic structure methods.

Time-dependent density functional theory (TDDFT) techniques are a promising alternative to multireference wave function-based electronic structure methods, and these have recently been used[18] in conjunction with surface hopping[57] methods for nonadiabatic dynamics. Unfortunately, the presently available TDDFT methods can only describe excited PESs in regions where the excited state of interest has single-excitation character relative to the ground state and furthermore fail to describe regions near conical intersections correctly.[58,59] Until these problems are rectified, TDDFT methods are of limited utility in photochemical applications.

The *ab initio* QM calculations presented here use the state-averaged complete active space self-consistent field (SA-CASSCF) method.[60,61] CASSCF is a multireference technique, representing the wave function as a full CI expansion in a limited number of orbitals around the Fermi level. State averaging is

employed to avoid variational bias to the ground state; orbitals and CI coefficients are varied to minimize the *average* (equally weighted) energy of several states, resulting in a balanced treatment of the states of interest. The CASSCF method does not provide an efficient means of recovering dynamic electron correlation effects, and thus, the validation procedure mentioned above is very important. Specifically, the number of electrons and orbitals in the active space as well as the number of states included in the averaging should be chosen to provide the correct ordering of states and, as far as possible, the correct relative energies of important points on the excited-state PES. As we have previously discussed,[10] this often leads to small active spaces because the errors in static and dynamic electron correlation have a tendency to cancel one another. When large active spaces are used, static correlation is almost completely recovered while dynamic correlation is completely neglected. The resulting imbalance often leads to a poor description of the global features of the excited-state PESs. Ultimately, one would obviously prefer to include both static and dynamic correlation effects explicitly, for example, with multireference second-order perturbation theory[62,63] (MS-CASPT2) or multi-reference configuration interaction (MRCI). We have carried out AIMS simulations at these levels,[9,64,65] but the computational expense presently limits one to rather small molecules and short time scales.

Semiempirical Electronic Structure. Many biological chromophores are too large for direct application of AIMS with *ab initio* treatment of the electronic structure. In these cases, semiempirical methods are an attractive alternative. As discussed above, descriptions of photochemistry with nonadiabatic events require an electronic wave function with multireference character, which traditional semiempirical theories do not provide. The floating occupation molecular orbital configuration interaction (FOMO-CI) method[33,66,67] describes multireference character very efficiently by appealing to an ensemble description. In FOMO-CI, the orbitals in the active space are optimized by a self-consistent field procedure in which the orbitals are allowed to have fractional occupation numbers while keeping the total number of electrons fixed. The partial occupation of all orbitals in the active space results in a better basis for the subsequent CI expansion, analogous to the improved virtual orbitals[68,69] used in *ab initio* methods. A CAS-CI expansion allowing all occupations of the electrons in the chosen active space is then performed without further orbital optimization.

Most existing parameter sets for semiempirical methods have been optimized for ground-state properties on the basis of single-reference electronic wave functions. Thus, one expects that reparameterization will be required and we have so far done this on a case by case basis. There are indications that the resulting parameters are transferable to some degree,[70] but this has yet to be explored in depth. The reparameterization proceeds through a simple optimization of a weighted sum of the differences between *ab initio* or possibly experimental values and the corresponding values from the semiempirical method. We generally use a small set of *ab initio* data in this reparameterization, such as vertical excitation energies (and electronic-state character) at ground-state minima and relative energies of MECIs and excited-state minima. Nevertheless, the semiempirical PESs obtained with this procedure show excellent agreement with the global *ab initio* surfaces.[70–72]

Initial Conditions and Equilibration. In solution phase simulations using *ab initio* methods for the QM region, a cluster of solvent molecules (the MM system) was randomly generated around the QM region. The MM energy was then minimized

with respect to the MM atom positions. The full system was then equilibrated by running dynamics while repeatedly sampling MM atom velocities from the Boltzmann distribution at 300 K. In order to avoid the computational expense of *ab initio* electronic structure calculations during equilibration, the internal structure of the QM region was held rigid. Electrostatic interactions between the QM and MM systems were approximated by periodic recalculation of the electronic wave function for the QM system. After equilibration, initial conditions for the QM system were sampled from the ground-state Wigner distribution, while conditions for the MM system were taken from the last time step of equilibration.

When the QM region was treated semiempirically, equilibration was performed using Brownian dynamics at 298 K (with a friction coefficient of 0.1 fs^{-1}) on the full ground-state QM/MM energy surface, requiring a QM calculation at each time step of equilibration. Initial conditions for excited-state dynamics were then taken from the final time step of equilibration.

Free Energy Profiles. Free energy profiles were constructed from umbrella sampling data[73−75] using the weighted histogram analysis method[73,76−80] (WHAM). For umbrella sampling, molecular dynamics on a single electronic state were run with harmonic biasing potentials along the coordinate of interest, and Grossfield's WHAM software package[81] was then used to reconstruct the underlying free energy surfaces.

Electronic Absorption Spectra. Electronic absorption spectra were computed using a simple semiclassical approximation:[82]

$$\sigma_{S_0 \to S_1}(\omega) \propto \omega^3 \int d\mathbf{R} \, |\Psi_0(\mathbf{R})|^2 |\mu_{S_0 \to S_1}(\mathbf{R})|^2 \delta(V_{S_1}(\mathbf{R}) - V_{S_0}(\mathbf{R}) - \hbar\omega) \quad (6)$$

where $\Psi_0(\mathbf{R})$ is the initial ground-state wave function, $\mu_{S_0 \to S_1}$ is the S_1/S_0 transition dipole moment, and $V_{S_1}(\mathbf{R})$ and $V_{S_0}(\mathbf{R})$ the S_1 and S_0 potential energy surfaces. This expression was evaluated by Monte Carlo sampling from the density $|\Psi_0(\mathbf{R})|^2$ (i.e., by generating a set of independent initial conditions as described above). $\mu_{S_0 \to S_1}(\mathbf{R})$ and $V_{S_1}(\mathbf{R})$ for each sample were then evaluated using the multistate[62] second-order perturbation theory (MS-CASPT2) correction[63] to the CAS wave function.

Results

Neutral GFP Chromophore in Solution. Green fluorescent protein (GFP), found in the jellyfish *Aequorea victoria*, is a highly versatile photoactive protein widely used in molecular and cell biology and in medicine.[83,84] The photodynamics of the GFP chromophore are known to be highly sensitive to its local environment. In the wild-type protein environment, the chromophore fluoresces, but this fluorescence is quenched by nonradiative decay when the protein environment is disrupted.[85]

In this section, we focus on the isolated and solvated dynamics of neutral *p*-hydroxybenzylidene-imidazolinone (HBI, Scheme 1), a model GFP chromophore. Our previous studies of the GFP chromophore demonstrate that SA-2-CAS(2,2)/6-31G calculations capture the qualitative features of the potential energy surface about important torsion angles, as compared to calculations including dynamic correlation energy for HBI.[30,86] Moreover, preliminary results show that CAS(2,2) calculations are consistent with results computed using larger active spaces.[87] All calculations for HBI described in this section employ electronic structure at the *ab initio* SA-2-CAS(2,2) level of theory with the 6-31G basis set. In the solvated case, the chromophore was solvated in a cluster of 300 TIP3P water molecules.

SCHEME 1
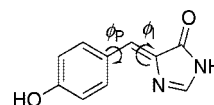
The photodynamics of HBI are initiated by a $\pi-\pi^*$ transition to S_1. In radiationless quenching from the S_1 to the ground state, the chromophore must undergo a large conformational change[88] involving twisting about the phenolate (P) or imidazolidinone (I) bridge bonds.[48] In the gas phase, the S_0 minimum is planar, with no torsion about the I and P bonds. The S_1 minimum is twisted about the I bridge bond, with ϕ_I near 90°.

Figure 1 shows the absorption spectra calculated from 100 Monte Carlo samples both in isolation and in aqueous solution. The results suggest a small blue shift in the spectrum upon solvation. While the gas phase spectrum of HBI has not been measured, Lammich et al. have estimated the absorption peak position of HBDI (a methylated variant of HBI, *vide infra*) in the gas phase.[89] They measured the spectrum of a cationic form of HBDI and then calculated the perturbation of the positively charged group with TDDFT to arrive at an estimate (399 nm) for the peak position of the neutral molecule in the gas phase. The absorption maximum of neutral HBDI in water has been measured[90] (372 nm), and these data imply a solvent-induced blue shift of 0.2 eV, in qualitative agreement with our results.

The dynamics of HBI after photoexcitation to S_1 were simulated using 20 AIMS starting trajectories, both in the gas phase and solvated in water. The excited-state population decay is shown in Figure 2. In the gas phase simulations, over half of the population remains in the excited state after 800 fs, while, in solution, we observe near total quenching to the ground state in just over 300 fs. The origin of this faster lifetime does not, as might be expected, arise solely from faster torsion. Indeed, as shown in Figure 3, the time scales for twisting around the I bridge bond range from 40−400 fs in the gas phase and from 40−250 fs in solution. The slight differences in the twisting time scales for the isolated and solvated molecules are insufficient to explain the nearly order-of-magnitude decrease in lifetime.

Much of the increase in quenching for the solvated molecule appears to be due to increased efficiency of nonadiabatic transitions after torsion about the I bridge bond. Figure 4 shows the decay of the S_1 population, but with the zero of time for each simulation shifted to the first time when the excited-state trajectory reaches a torsion about the I bridge bond of 70°. In solution, quenching to S_0 is rapid and efficient, completing within 100 fs after the molecule twists. However, in isolation,
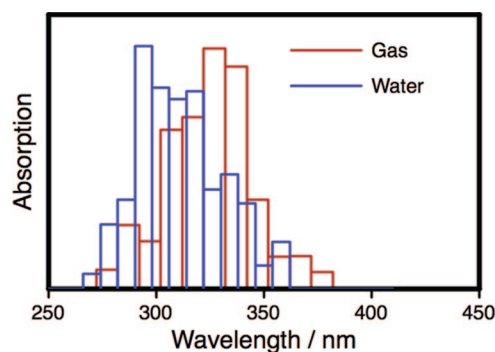
Figure 1. Calculated absorption spectra for the GFP chromophore in vacuum (red) and in aqueous solution (blue) from 100 Monte Carlo samples of the ground-state density.
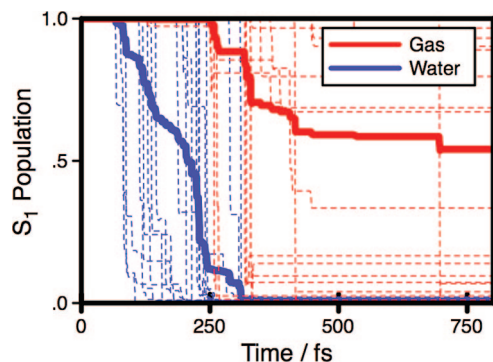
Centennial Feature Article

J. Phys. Chem. B, Vol. 113, No. 11, 2009 **3285**

Figure 2. Total population (solid lines) and population for each trajectory (dashed lines) on S_1 for HBI in vacuum (red) and in solution (blue). Aqueous solvation greatly accelerates quenching to the ground state in HBI.
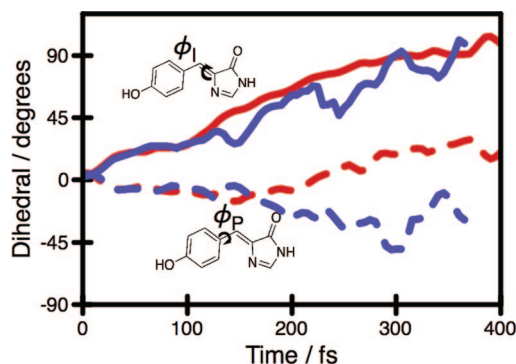

Figure 3. I (solid line) and P (dashed) dihedral angles as a function of time in both isolation (red) and solution (blue). The time scales for torsion are similar in both cases.
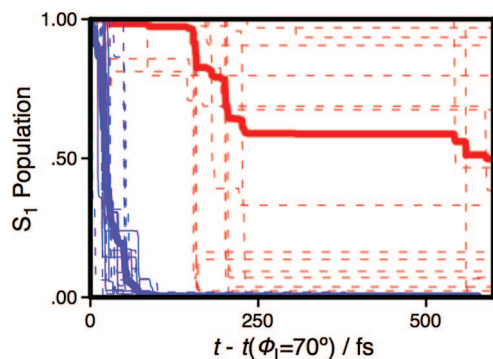

Figure 4. S_1 population as a function of time, where the individual trajectories have been adjusted such that the zero of time represents the point in the trajectory where the GFP chromophore reaches a twisted configuration ($\phi_I = 70°$). Once the molecule is twisted, population transfer is very rapid and efficient in solution (blue), while in the gas phase (red) there is still significant variability in the population dynamics. This is consistent with the presence of a true twisted minimum in the gas phase lying below the S_1/S_0 MECI.

nearly half of the population remains in S_1 even 600 fs after reaching a twisted geometry. This strongly suggests that the S_1/S_0 MECI lies above the S_1 minimum in the isolated molecule such that there is an effective barrier to reach the MECI. This behavior has been observed in our previous semiempirical QM/MM simulations[30,86] of HBI, and the present results confirm that the behavior is due to solvent stabilization of the S_1/S_0 MECI. In particular, the S_0/S_1 MECI becomes the lowest energy geometry in S_1 in the aqueous environment, while there is a well-defined twisted minimum in S_1 in the isolated chromophore. Minimizations carried out from geometries where nonadiabatic
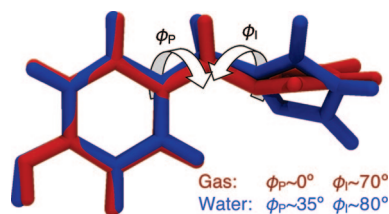

Figure 5. Overlay of gas phase (red) and solution phase (blue) MECIs; the solution MECI is also the lowest energy point on the S_1 PES.
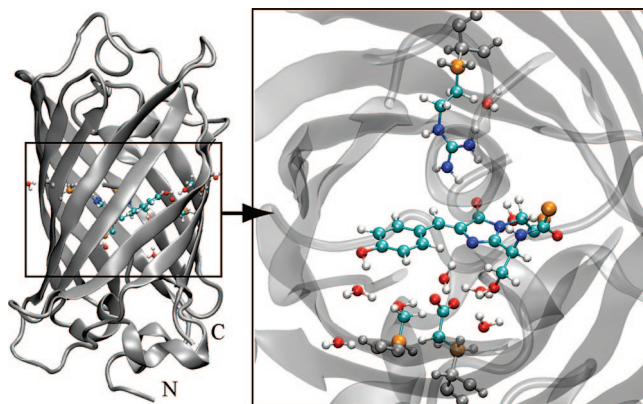

Figure 6. Green fluorescent protein is a β-barrel surrounding the chromophore (left). Atoms modeled classically are shown in gray ball-and-stick and ribbon representation (right, from top of left figure). QM atoms are presented in color-coded ball-and-stick representation (white, hydrogen; red, oxygen; blue, nitrogen; cyan, carbon). Connection atoms are shown in orange.

transitions occur in the solution phase AIMS simulations support this idea. Figure 5 shows both the gas phase MECI and a solution phase MECI. While there is a well-defined S_1 minimum in the isolated chromophore, such a minimum could not be located in the solvated environment, suggesting that the S_0/S_1 MECI is the lowest energy structure in solution. The solvated CI is shifted geometrically as well as energetically, involving torsion about both the P and I bonds (instead of just the I bond in the gas phase).

Neutral GFP Chromophore in Protein. 4-Hydroxyben-zylidene-1,2-dimethylimidazolinone (HBDI), another model GFP chromophore, has a fluorescence quantum yield of only 10^{-3} in solution, but the yield jumps to 0.8 for the wild-type GFP.[85] The lifetimes of the excited states of both the neutral and anionic forms of HBDI were measured to be 1.2 ps in solution,[88] dramatically shorter than the fluorescence lifetime of $\approx$3 ns observed in the protein environment.[84] We have investigated the mechanism by which the protein suppresses radiationless quenching of the neutral excited state, thereby enhancing the fluorescence quantum yield. As shown in Figure 6, our dynamics simulations of the full GFP protein modeled the QM region (the chromophore, Arg92, Ser205, Glu223, and eight water molecules) using reparameterized semiempirical FOMO-CI.[33,66,67] The remaining 223 residues and 155 water molecules comprised the MM region; in the solvated case, the chromophore was embedded in a cluster of 150 water molecules. Covalent links between the two systems were treated using connection atoms.[48,49]

Dynamics simulations in the protein environment reveal relatively small variation of P and I torsion angles, showing that the chromophore tends to maintain its planar shape over at least several picoseconds, in contrast to the subpicosecond twisting observed in solution. We therefore used umbrella sampling to construct a free energy profile for twisting of the
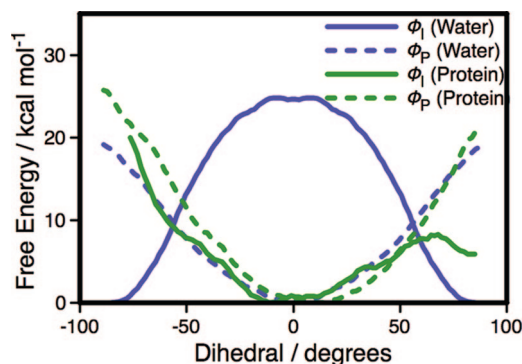
Figure 7. Free energy as a function of torsion around the I (solid) and P (dashed) in water (blue) and protein (green) environments, calculated using umbrella sampling on the semiempirical QM/MM surfaces. While torsion about I is energetically favorable in solution, there is an approximately 7 kcal/mol barrier in the protein.

chromophore in the S_1 excited state, in both protein and solution environments. As shown in Figure 7, the calculated free energy profiles display a barrier to torsion about the P bridge bond in both solvent and protein. However, in the protein environment, there is also a barrier to torsion about the I bridge bond which is not present in solution. The origin of this barrier is currently under investigation, but it is clearly the mechanism by which the structure of the protein cavity prevents radiationless quenching and thereby facilitates the observed *in vivo* fluorescence of GFP.

PYP Chromophore in Solution. The photoactive yellow protein (PYP) is a cytoplasmic blue light photoreceptor which initiates the negative phototaxis pathway of *Halorhodospira halophila*.[91] Upon photoabsorption, *trans*-to-*cis* isomerization of the chromophore initiates the photocycle of PYP,[92,93] which culminates in a partial unfolding of the protein. Several theoretical[94−96] studies have suggested that the local environment of the chromophore, *p*-coumaric acid or **pCA**, plays a determinative role in its excited-state dynamics. The chromophore is linked via a thioester bond to the unique cysteine in the protein and is thought to be deprotonated in ground-state PYP.[91,97] The photodynamics of several models of **pCA** have been experimentally characterized both in gas phase[98,99] and in solution.[100−107] In the various solution phase experimental[105,107] and theoretical[96,108−113] studies, rotations of the ethylenic double bond (D) and the phenyl-adjacent single bond (S) were proposed as possible reaction coordinates for dynamics on the excited state.

We have carried out AIMS simulations of an anionic model of the chromophore, *p*-hydroxybenzylidene acetone (**pCK−**), depicted in Scheme 2. Electronic structure calculations for **pCK−** were at the SA2-CAS(8/6) level of theory with the 6-31G* basis set. In solution phase simulations, the chromophore was embedded in a cluster of 300 TIP3P water molecules. The electronic absorption spectrum for **pCK−**, calculated with 100 samples for each of the solution and gas phase cases, is shown in Figure 8. Although the spectra themselves are red-shifted from experimental values by about 0.5 eV in each case, the calculations do capture a blue shift of approximately 0.5 eV in solution relative to the gas phase. This blue shift is consistent with estimates by Zewail and co-workers.[98,107]
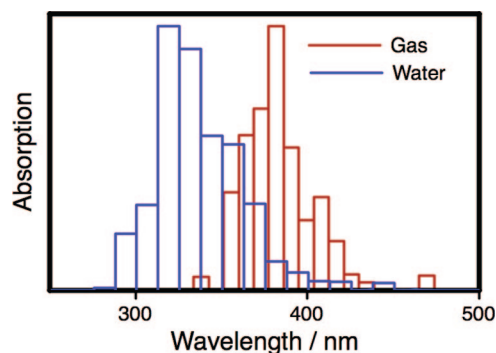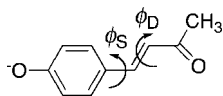
SCHEME 2

Figure 8. Electronic absorption spectrum of PYP chromophore in the gas phase (red) and solution (blue) PYP, computed from 100 samples each. We observe a solvent-induced blue-shift, from ∼390 to 310 nm, the magnitude of which is consistent with experiment.
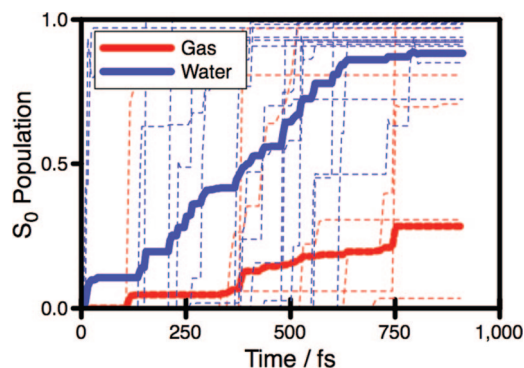

Figure 9. Ground-state population of the model PYP chromophore over 900 fs of FMS dynamics in solution (blue) and in the gas phase (red). Solid lines are the proportion of total population transferred; dashed lines indicate the ground-state population for each trajectory. Quenching to the electronic ground state is much faster in the solvated environment compared to the gas phase.

Our simulations suggest that solvation has a dramatic effect on the excited-state dynamics of **pCK−**. As in the case of GFP chromophore, the solvated dynamics exhibit a marked decrease in excited-state lifetime, with most of the solvated initial trajectories transferring their population to the ground state within 1 ps, as shown in Figure 9. This shortened lifetime appears slightly faster than the fluorescence decay of 1.3 ± 0.5 ps observed in time-resolved fluorescence up-conversion experiments.[107]

The dynamics also suggest a shift and stabilization of the S_1/S_0 conical intersections in solution. Figure 10 shows population transfer events from each S_1 trajectory as a function of torsion about the phenyl-adjacent (S) and ethylenic (D) bonds. The plot reveals two major intersections in each phase: the first group of events (around $\phi_D = 60°$ and $\phi_S = 0$ or 180°) correspond to a purely D-twisted intersection, and the second group of events (circled) correspond to an S-twisted intersection. In the gas phase, the S-twisted intersection involves torsion about both the S and D bonds, but, in solution, this intersection is purely S-twisted. This shift in geometry also appears to be accompanied by an energetic stabilization: energy minimizations of **pCK−** on S_1 suggest that both the S-twisted and D-twisted CIs are locally the lowest energy points on S_1 in solution, but not in the gas phase. Solvent stabilization of these intersections accounts for the vastly shorter lifetime of **pCK−** in aqueous solution as compared to the gas phase.

Electrostatic Control of the PYP Chromophore. While in GFP the protein environment effectively blocks the nonradiative decay pathway of the chromophore, it has been suggested that

Centennial Feature Article

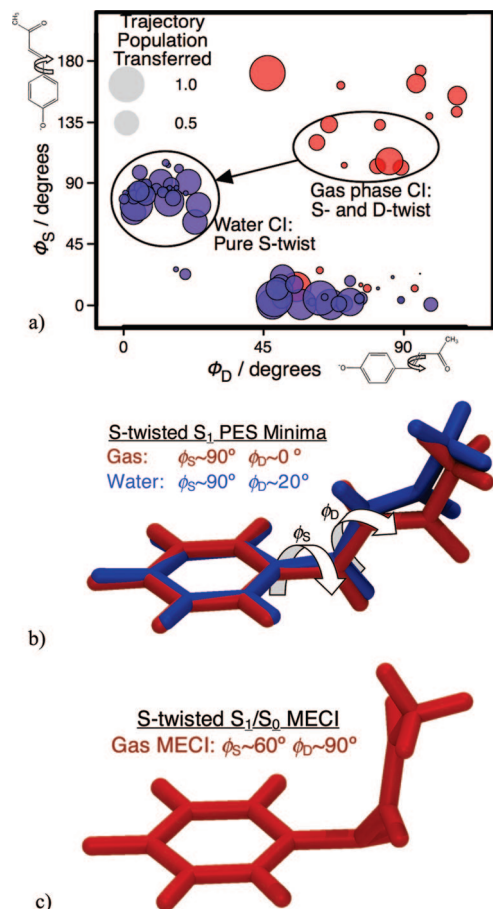*J. Phys. Chem. B, Vol. 113, No. 11, 2009* **3287**

Figure 10. (a) Population transfer as a function of S and D torsion angles, for water-solvated (blue) and gas phase (red) simulations. Each bubble represents a spawning event; bubble size indicates the amount of population transferred to the ground state. There is significantly more population transfer in the solvated case, and the position of one of the conical intersections shifts from both S- and D-twisted to purely S-twisted (circled). (b) Overlay of the gas phase S-twisted S_1 PES minimum (red) and a similar solvated minimum (blue). The solvated geometry is an S_1/S_0 conical intersection as well as the lowest energy geometry on S_1; this stabilization of the intersection facilitates efficient quenching to the ground state. (c) In contrast, the gas phase S-twisted MECI is not a minimum on the PES, and requires both single and double bond torsion.

the electrostatic environment surrounding the chromophore in PYP both enhances and directs its internal conversion process. In particular, the positively charged Arg52 residue in wild-type PYP lies in close proximity to the chromophore, is highly conserved, and creates a significant electric field in the binding pocket. We have previously reported that electrostatic interactions with a positive point charge could control the photoproducts of the isolated anionic PYP chromphore, leading to *trans-to-cis* (i.e., double bond) isomerization, as observed in the native PYP.[95] Robb and co-workers found similar effects in their QM/MM dynamics simulations with explicit representations of several residues surrounding the chromophore:[94] they showed that the positively charged Arg52 residue induces significant bias toward double bond isomerization, as compared to a mutant with a neutral residue.

Figure 11 shows two representative AIMS dynamics simulations of **pCK⁻** in the presence of a point charge, computed with the same electronic structure method as used in the simulations of solvated **pCK⁻** discussed above. The point charge was placed at the location of the terminal nitrogen atom of Arg52, as given in the crystal structure.[114] The magnitude of
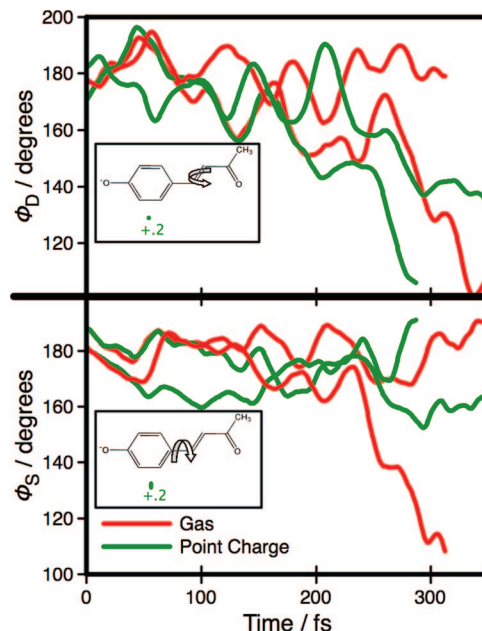

Figure 11. Time evolution of the two dihedral angles, D (upper pane) and S (lower pane), from four representative AIMS runs, two in the gas phase (red) and two in the presence of a positive point charge (green). Gas phase trajectories show torsion about both the D and S bonds, while those with the point charge isomerize exclusively around D.
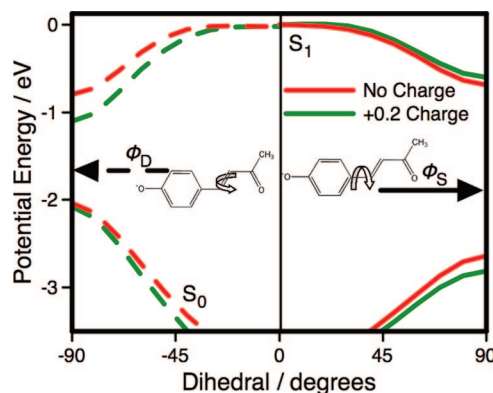

Figure 12. S_0 and S_1 potential energy curves computed using SA-2-CAS(8/6) with the 6-31G* basis set for the model anionic PYP chromophore, both isolated (red) and in the presence of a point charge (green). Traces shown are for rigid torsion about D (dashed, to the left) and S (solid, to the right). In each case, the bond lengths are set to those at the corresponding optimized twisted S_1 minimum of the isolated molecule. The zero of energy is at the planar geometry that has bond lengths of the single bond twisted S_1 minimum. The double bond torsion is favored by a positive point charge, which also reduces the S_0/S_1 energy gap at the double bond twisted S_1 minimum geometry.

the point charge was chosen such that the localized charge environment is a minimal perturbation to the isolated molecule (for example, in terms of excitation energies and oscillator strengths of the excited states), and simulations were carried out for both positive and negative charges. In our simulations, the +0.20 point charge suppresses single bond torsion while promoting double bond torsional motion. The −0.20 charge does the opposite, promoting single bond torsion and suppressing double bond torsion. These electrostatic effects on torsional relaxation are clearly seen in the S_1 PESs shown in Figure 12 for **pCK⁻** in isolation and in the presence of the positive charge. Note that the electrostatic effects do not play a significant role for torsions about either bond until rotation through ap-

3288 *J. Phys. Chem. B, Vol. 113, No. 11, 2009*

Virshup et al.

proximately 30° of torsion. The PES is quite flat with respect to torsion in both isolation and point charge environments. One can thus define a value of the torsion which is a "point of no return" for torsion about either bond, and the dynamics consist of torsional fluctuations about both of the S and D bonds until this critical torsion is reached. The main effect of the positive point charge is to lower this critical angle for torsion about the double bond while (slightly) raising the critical angle for torsion about the single bond. Thus, the **pCK⁻** chromophore in isolation is precariously perched between the two outcomes (S and D torsion), which is an ideal situation for allowing subtle effects in the environment to completely alter the branching ratio between outcomes. Therefore, the initial excited-state dynamics are not significantly different in the various environments. Once isomerized, however, the positive point charge environment also reduces the S_0/S_1 energy gap at the double bond twisted S_1 minimum, increasing both the efficiency and rate of radiationless decay to S_0.

Retinal Protonated Schiff Base in Solution and Rhodopsin. Rhodopsin, the low-light photoreceptor in vertebrate retina, belongs to the G-protein-coupled receptor (GPCR) family. The chromophore in rhodopsin is 11-*cis* retinal protonated Schiff base (RPSB), as depicted with some of its photoproducts in Scheme 3. When triggered by light, the chromophore undergoes *cis−trans* isomerization, leading to a protein-wide conformational change that initiates the visual perception pathway. This very efficient photomechanical energy conversion process is a result of the ultrafast isomerization (less than 200 fs) of RPSB and its high quantum yield (0.67).[115]

SCHEME 3
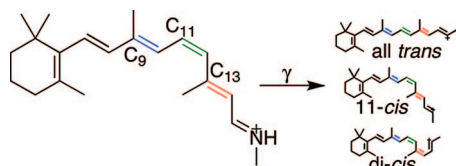
In the simulations presented here, RPSB was treated with the semiempirical FOMO-CI method[33,66,67] using reoptimized parameters.[72] In the gas phase and solvated simulations, an analog without the beta-ionone ring was used. In the methanol-solvated case, all methanol molecules were part of the MM
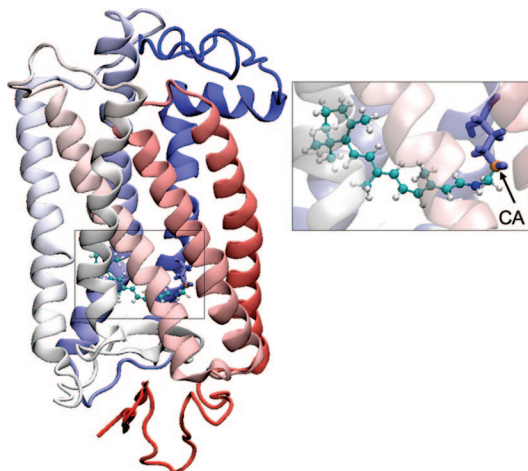
Figure 13. Model of rhodopsin for QM/MM simulations. The QM RPSB is in ball-and-stick representation, and the MM region is in ribbon cartoon representation. The close-up shows the connection atom (CA) in orange.
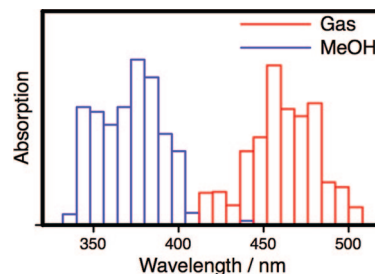
Figure 14. Calculated absorption spectra for ground-state 11-*cis* RPSB in vacuum (red) and solvated in MeOH (blue). The solvation blue-shift of ∼0.6 eV here is similar to that observed in experiment.
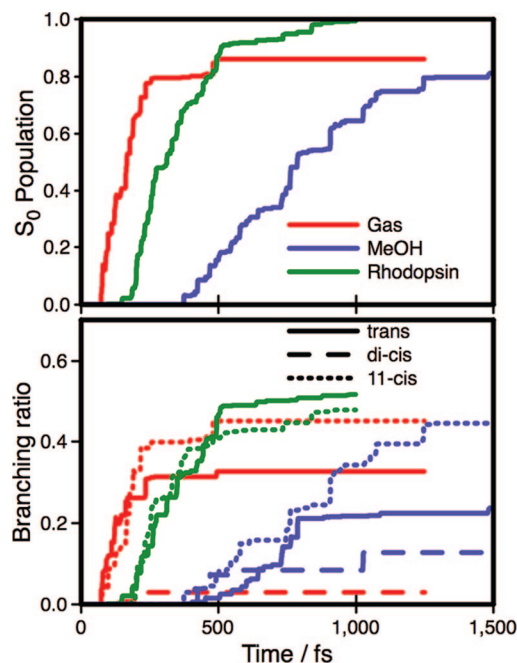
Figure 15. Upper panel: Proportion of population quenching from S_1, from 15−20 trajectories each in the gas phase (red), MeOH solvated (blue), and in the rhodopsin protein (green). In this case, the population transfer rate is retarded by both the solvent and protein environments. Lower panel: RPSB branching ratios for the *trans* (solid line), di-*cis* (dashed), and unisomerized 11-*cis* (dotted) photoproducts. The branching ratios appear similar in both solution and gas phase. The rhodopsin environment enhances the quantum yield of the *trans* isomer as well as eliminating the various di-*cis* photoproducts.

system. As depicted in Figure 13, in the rhodopsin protein environment, RPSB was connected to the rest of the protein (the MM system) via a connection atom at C_δ of Lys296 with connection parameters from Toniolo et al.[48] All surrounding residues are treated within the molecular mechanics framework, including the counterion Glu113. The residue Glu181 is treated in its neutral form, in accord with previous theoretical work[116] and experimental evidence.[117,118] However, we alert the reader that the ionization state of the Glu181 residue remains a point of some controversy.[119,120] The electrostatic influence of the surrounding residues is thus included in the model, but excited states involving charge transfer between the surrounding residues and RPSB are of course excluded from consideration and are not expected to be of significant importance. The rhodopsin geometry was based on chain A of the crystal structure of bovine rhodopsin.[121] All trajectories began with RPSB in the 11-*cis* conformation.

The peak of the calculated absorption spectrum for 11-*cis* RPSB (Figure 14) shifts by approximately 0.6 eV upon solvation in MeOH. While, again, the absolute position of the peak is
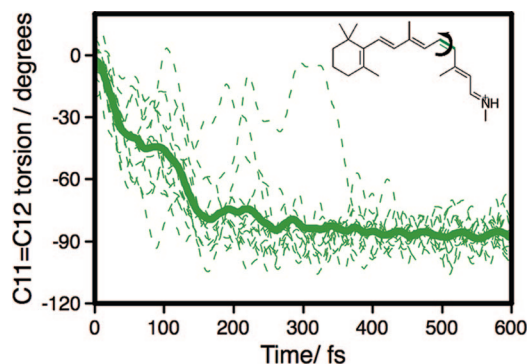
Centennial Feature Article

J. Phys. Chem. B, Vol. 113, No. 11, 2009 **3289**

Figure 16. C11=C12 torsion angle after photoexcitation for 11-*cis* RPSB in rhodopsin, average (solid line) and for each trajectory (dashed). All trajectories undergo this torsion, leading to a more specific and efficient reaction than in the disordered environments.

shifted by 0.5 eV relative to experiment, the calculated solvation blue shift is in good agreement with the experimental value of 0.8 eV,[122,123] especially considering the low level of electronic structure theory employed.

The ground-state population transferred from S_1 for RPSB in isolation, methanol, and protein environments is shown in the upper panel of Figure 15. In contrast to the chromophores of GFP and PYP, the excited-state lifetime of RPSB is shorter in isolation than it is in methanol solution or rhodopsin protein. Despite the difference in lifetime, we find the product branching ratio to be roughly the same in both solution and isolation, as shown in the lower panel of Figure 15. In both isolation and solution, the dominant product is unisomerized 11-*cis*, followed by *trans*-RPSB and small quantities of various di-*cis* isomers.

In contrast to the gas phase and solution environments, RPSB shows highly directed dynamics in the rhodopsin environment, with our simulation showing a higher yield and more specific reaction products. When excited to S_1, nearly all trajectories immediately begin to twist around the $C_{11}=C_{12}$ bond, as shown in Figure 16. After torsion to 90°, the trajectories quickly begin population transfer to the ground state. More than half of the population forms distorted all-*trans* RPSB, which may be tentatively identified with the transient photorhodopsin photoproduct;[115,124] the remaining population reverts to the original 11-*cis* configuration. As opposed to the gas phase and solvated environments, no secondary di-*cis* photoisomers are observed. It appears that the local structure of rhodopsin has a role in directing this reaction; the binding pocket is somewhat tight, implying minimal volume change during isomerization. In the simulations, this minimal volume isomerization is achieved by concerted rotations of about 20° of the neighboring bonds flanking the $C_{11}=C_{12}$ bond (not shown here).

Discussion

We have combined both *ab initio* and semiempirical electronic structure methods with MM force fields to investigate the photochemical dynamics of several different chromophores in isolated, solvated, and protein environments. Even in disordered solution, the environment plays an important role in dynamics. For both the GFP and PYP chromophores, we observe solvent stabilization of conical intersection geometries, leading to dramatically shorter lifetimes than in the gas phase. In contrast, the methanol solution environment serves to slow the reaction in 11-*cis* RPSB, although we find little difference in the final product ratios in isolated and solution environments. The native protein environment of each chromophore is also seen to play a role in directing its photodynamics. In the case

of GFP, structural effects from the protein create a strong barrier to isomerization on the excited state, preventing nonradiative decay and thereby enhancing its fluorescence by several orders of magnitude. In contrast, the electrostatic environment of PYP stabilizes and directs internal conversion of its chromophore, enhancing the production of a particular photoisomer. Rhodopsin also biases and enhances the internal conversion of RPSB toward a single photoisomer but, like GFP, appears to do so through a structural mechanism.

The QM/MM scheme presented here is, in some respects, the simplest possible coupling of QM and MM methods, and treatment of the QM/MM interaction involves several implicit approximations. For electrostatic interactions between the QM and MM regions, the fixed-charge force fields employed in our calculations are inflexible. It would be desirable to incorporate polarizable force fields and/or charge transfer models in order to describe environmental reactions to the photoinduced change in the solute charge distribution. In this scheme, too, van der Waals interactions between QM and MM regions, an inherently electronic phenomenon, are described without reference to the electronic wave function. We have previously suggested an electronic wave function-based approach to modeling the Pauli repulsion term in the Lennard-Jones energy by associating a model wave function with the MM system.[125] This approach has been simplified by using pseudopotentials in recent work, and in that context, it can also provide an improved description of bonding across the QM/MM boundary.[50] We are incorporating these improvements to the QM/MM methodology into our AIMS dynamics approach and expect that these will lead to more accurate and more efficient simulations.

References and Notes

(1) Zewail, A. H. *J. Phys. Chem. A* **2000**, *104*, 5660.
(2) Yarkony, D. R. *Rev. Mod. Phys.* **1996**, *68*, 985.
(3) Yarkony, D. R. *Acc. Chem. Res.* **1998**, *31*, 511.
(4) Bernardi, F.; Olivucci, M.; Robb, M. A. *Chem. Soc. Rev.* **1996**, *25*, 321.
(5) Klessinger, M.; Michl, J. *Excited States and Photochemistry of Organic Molecules*; VCH Publishers, Inc.: New York, 1995.
(6) Matsika, S.; Yarkony, D. R. *J. Am. Chem. Soc.* **2003**, *125*, 10672.
(7) Matsika, S.; Yarkony, D. R. *J. Am. Chem. Soc.* **2003**, *125*, 12428.
(8) Matsika, S. *J. Phys. Chem. A* **2005**, *109*, 7538.
(9) Coe, J. D.; Martinez, T. J. *J. Am. Chem. Soc.* **2005**, *127*, 4560.
(10) Coe, J. D.; Martinez, T. J. *J. Phys. Chem. A* **2006**, *110*, 618.
(11) Martinez, T. J. *Chem. Phys. Lett.* **1997**, *272*, 139.
(12) Manaa, M. R.; Yarkony, D. R. *J. Chem. Phys.* **1993**, *99*, 5251.
(13) Bearpark, M. J.; Robb, M. A.; Schlegel, H. B. *Chem. Phys. Lett.* **1994**, *223*, 269.
(14) Sicilia, F.; Blancafort, L.; Bearpark, M. J.; Robb, M. A. *J. Chem. Theory Comput.* **2008**, *4*, 257.
(15) Sicilia, F.; Bearpark, M. J.; Blancafort, L.; Robb, M. A. *Theor. Chem. Acc.* **2007**, *118*, 241.
(16) Migani, A.; Robb, M. A.; Olivucci, M. *J. Am. Chem. Soc.* **2003**, *125*, 2804.
(17) Laino, T.; Passerone, D. *Chem. Phys. Lett.* **2004**, *389*, 1.
(18) Tapavicza, E.; Tavernelli, I.; Rothlisberger, U. *Phys. Rev. Lett.* **2007**, *98*, 023001.
(19) Ben-Nun, M.; Quenneville, J.; Martínez, T. J. *J. Phys. Chem. A* **2000**, *104*, 5161.
(20) Martinez, T. J. *Acc. Chem. Res.* **2006**, *39*, 119.
(21) Frutos, L. M.; Andruniow, T.; Santoro, F.; Ferre, N.; Olivucci, M. *Proc. Natl. Acad. Sci.* **2007**, *104*, 7764.
(22) Weingart, O.; Schapiro, I.; Buss, V. *J. Phys. Chem. B* **2007**, *111*, 3782.
(23) Levine, B. G.; Martinez, T. J. *Annu. Rev. Phys. Chem.* **2007**, *58*, 613.
(24) Kim, M. H.; Shen, L.; Tao, H.; Martinez, T. J.; Suits, A. G. *Science* **2007**, *315*, 1561.

(25) Barbatti, M.; Ruckenbauer, M.; Szymczak, J. J.; Aquino, A. J. A.; Lischka, H. *Phys. Chem. Chem. Phys.* **2008**, *10*, 482.

(26) van der Horst, M. A.; Hellingwerf, K. J. *Acc. Chem. Res.* **2004**, *37*, 13.

(27) Balzani, V.; Clemente-Leon, M.; Credi, A.; Ferrer, B.; Venturi, M.; Flood, A. H.; Stoddart, J. F. *Proc. Natl. Acad. Sci.* **2006**, *103*, 1178.

(28) Morin, J.; Shirai, Y.; Tour, J. M. *Org. Lett.* **2006**, *8*, 1713.

(29) Fortin, D. L.; Banghart, M. R.; Dunn, T. W.; Borges, K.; Wagenaar, D. A.; Gaudry, Q.; Karokossian, M. H.; Otis, T. S.; Kristan, W. B.; Trauner, D.; Kramer, R. H. *Nat. Methods* **2008**, *5*, 331.

(30) Toniolo, A.; Olsen, S.; Manohar, L.; Martinez, T. J. *Faraday Discuss.* **2004**, *127*, 149.

(31) Burghardt, I.; Cederbaum, L. S.; Hynes, J. T. *Faraday Discuss.* **2004**, *127*, 395.

(32) Schaefer, L. V.; Groenhof, G.; Boggio-Pasqua, M.; Robb, M. A.; Grubmueller, H. *PLoS Comput. Biol.* **2008**, *4*, e10000034.

(33) Toniolo, A.; Granucci, G.; Martinez, T. J. *J. Phys. Chem. A* **2003**, *107*, 3822.

(34) Hayashi, S.; Tajkorshid, E.; Schulten, K. *Biophys. J.* **2003**, *85*, 1440.

(35) Losa, A. M.; Martin, M. E.; Galvan, J. F.; Aguilar, M. A. *Chem. Phys. Lett.* **2007**, *443*, 76.

(36) Yamazaki, S.; Kato, S. *J. Chem. Phys.* **2005**, *123*, 114510.

(37) Burghardt, I.; Hynes, J. T. *J. Phys. Chem. A* **2006**, *110*, 11411.

(38) Ben-Nun, M.; Martínez, T. J. *Adv. Chem. Phys.* **2002**, *121*, 439.

(39) Heller, E. J. *J. Chem. Phys.* **1981**, *75*, 2923.

(40) Werner, H.-J.; Knowles, P. J.; Lindh, R.; Schuetz, M.; Celani, P.; Korona, T.; Manby, F. R.; Rauhut, G.; Amos, R. D.; Bernhardsson, A.; Berning, A.; Cooper, D. L.; Deegan, M. J. O.; Dobbyn, A. J.; Eckert, F.; Hampel, C.; Hetzer, G.; Lloyd, A. W.; McNicholas, S. J.; Meyer, W.; Mura, M. E.; Nicklass, A.; Palmieri, P.; Pitzer, R.; Schumann, U.; Stoll, H.; Stone, A. J.; Tarroni, R.; Thorsteinsson, T. *MOLPRO*, version 2006.1, a package of ab initio programs, 2006.

(41) Stewart, J. J. P. *MOPAC 2002*; Fujitsu Limited: Tokyo, Japan, 1999.

(42) Levine, B. G.; Coe, J. D.; Virshup, A. M.; Martínez, T. J. *Chem. Phys.* **2008**, *347*, 3.

(43) Warshel, A.; Levitt, M. *J. Mol. Biol.* **1976**, *103*, 227.

(44) Field, M.; Bash, P.; Karplus, M. *J. Comput. Chem.* **1990**, *11*, 700.

(45) Gao, J. L. *Acc. Chem. Res.* **1996**, *29*, 298.

(46) Friesner, R. A.; Guallar, V. *Annu. Rev. Phys. Chem.* **2005**, *56*, 389.

(47) Singh, U. C.; Kollman, P. A. *J. Comput. Chem.* **1986**, *7*, 718.

(48) Toniolo, A.; Ciminelli, C.; Granucci, G.; Laino, T.; Persico, M. *Theor. Chim. Acta* **2004**, *111*, 270.

(49) Antes, I.; Thiel, W. *J. Phys. Chem. A* **1999**, *103*, 9290.

(50) Slavíček, P.; Martínez, T. J. *J. Chem. Phys.* **2006**, *124*, 084107.

(51) Cornell, W.; Cieplak, P.; Bayly, C.; Gould, I.; Merz, J. K.; Ferguson, D.; Spellmeyer, D.; Fox, T.; Caldwell, J.; Kollman, P. *J. Am. Chem. Soc.* **1995**, *117*, 5179.

(52) Weiner, S. J.; Kollman, P. A.; Case, D. A.; Singh, U. C.; Ghioand, C.; Alagona, G., Jr.; Weiner, P. *J. Am. Chem. Soc.* **1984**, *106*, 765.

(53) Cheatham, T. E., III; Cieplak, P.; Kollman, P. A. *J. Biomol. Struct. Dyn.* **1999**, *16*, 845.

(54) Jorgensen, W. L.; Chandrasekhar, J.; Madura, J. D.; Impey, R. W.; Klein, M. L. *J. Chem. Phys.* **1983**, *79*, 926.

(55) Jorgensen, W. L.; Maxwell, D. S.; Tirado-Rives, J. *J. Am. Chem. Soc.* **1996**, *118*, 11225.

(56) Olsen, S.; Toniolo, A.; Ko, C.; Manohar, L.; Lamothe, K.; Martinez, T. J. Computation of Reaction Mechanisms and Dynamics in Photobiology. In *Computational Photochemistry*; Olivucci, M., Ed.; Elsevier: Amsterdam, 2005.

(57) Tully, J. C. *J. Chem. Phys.* **1990**, *93*, 1061.

(58) Levine, B. G.; Ko, C.; Quenneville, J.; Martínez, T. J. *Mol. Phys.* **2006**, *104*, 1039.

(59) Cordova, F.; Doriol, J.; Ipatov, A.; Casida, M. E.; Fillippi, C.; Vela, A. *J. Chem. Phys.* **2007**, *127*, 164111.

(60) Docken, K. K.; Hinze, J. *J. Chem. Phys.* **1972**, *57*, 4928.

(61) Roos, B. O. *Adv. Chem. Phys.* **1987**, *69*, 399.

(62) Finley, J.; Malmqvist, P.-A.; Roos, B. O.; Serrano-Andres, L. *Chem. Phys. Lett.* **1998**, *288*, 299.

(63) Roos, B. O. *Acc. Chem. Res.* **1999**, *32*, 137.

(64) Quenneville, J.; Ben-Nun, M.; Martinez, T. J. *J. Photochem. Photobiol., A* **2001**, *144*, 229.

(65) Ben-Nun, M.; Martinez, T. J. *Chem. Phys. Lett.* **1998**, *290*, 289.

(66) Granucci, G.; Toniolo, A. *Chem. Phys. Lett.* **2000**, *325*, 79.

(67) Toniolo, A.; Ben-Nun, M.; Martínez, T. J. *J. Phys. Chem. A* **2002**, *106*, 4679.

(68) Potts, D. M.; Taylor, C. M.; Chaudhuri, R. K.; Freed, K. F. *J. Chem. Phys.* **2001**, *114*, 2592.

(69) Harding, L. B.; Goddard, W. A. *J. Am. Chem. Soc.* **1977**, *99*, 677.

(70) Toniolo, A.; Levine, B.; Thompson, A.; Quenneville, J.; Ben-Nun, M.; Owens, J.; Olsen, S.; Manohar, L.; Martinez, T. J. Photochemistry from First Principles and Direct Dynamics. In *Computational Methods in Organic Photochemistry*; Kutateladze, A., Ed.; Marcel-Dekker: New York, 2005.

(71) Toniolo, A.; Thompson, A. L.; Martínez, T. J. *Chem. Phys.* **2004**, *304*, 133.

(72) Owens, J. M.; Punwong, C.; Martínez, T. J. A Re-Optimized PM3-Based Parameter Set for Retinal Protonated Schiff Base, in preparation.

(73) Frenkel, D.; Smit, B. *Understanding molecular dynamics: from algorithms to applications*; Academic Press: San Diego, CA, 1995.

(74) Torrie, G. M.; Valleau, J. P. *Chem. Phys. Lett.* **1974**, *28*, 578.

(75) Torrie, G. M.; Valleau, J. P. *J. Comput. Phys.* **1977**, *23*, 187.

(76) Ferrenberg, A. M.; Swendsen, R. H. *Phys. Rev. Lett.* **1988**, *61*, 2635.

(77) Ferrenberg, A. M.; Swendsen, R. H. *Phys. Rev. Lett.* **1989**, *63*, 1195.

(78) Kumar, S.; Bouzida, D.; Swendsen, R. H.; Kollman, P. A.; Rosenberg, J. M. *J. Comput. Chem.* **1992**, *13*, 1011.

(79) Kumar, S.; Rosenberg, J. M.; Bouzida, D.; Swendsen, R. H.; Kollman, P. A. *J. Comput. Chem.* **1995**, *16*, 1339.

(80) Roux, B. *Comput. Phys. Commun.* **1995**, *91*, 275.

(81) Grossfield, A. *WHAM*, version 2.0.2; 2007.

(82) Schinke, R. *Photodissociation Dynamics*; Cambridge University Press: Cambridge, U.K., 1995.

(83) Zimmer, M. *Chem. Rev.* **2002**, *102*, 759.

(84) Tsien, R. Y. *Annu. Rev. Biochem.* **1998**, *67*, 509.

(85) Niwa, H.; Inouye, S.; Hirano, T.; Matsuno, T.; Kojima, S.; Kubota, M.; Ohashi, M.; Tsuji, F. I. *Proc. Natl. Acad. Sci.* **1996**, *93*, 13617.

(86) Toniolo, A.; Olsen, S.; Manohar, L.; Martinez, T. J. Ultrafast Excited State Dynamics in Green Fluorescent Protein Chromophore. In *Ultrafast Molecular Events in Chemistry and Biology: Femtochemistry VI*; Martin, M., Hynes, J. T., Eds.; Elsevier: Amsterdam, 2004.

(87) Olsen, S. C. The Electronic Excited States of Green Fluorescent Protein Chromophore Models, University of Illinois at Urbana-Champaign, PhD Thesis, 2004.

(88) Usman, A.; Mohammed, O. F.; Nibbering, E. T. J.; Dong, J.; Solntsev, K. M.; Tolbert, L. M. *J. Am. Chem. Soc.* **2005**, *127*, 11214.

(89) Lammich, L. M.; Petersen, M. Å.; Nielsen, M. B.; Anderson, L. H. *Biophys. J.* **2007**, *92*, 201.

(90) Dong, J.; Solnstev, K. M.; Tolbert, L. M. *J. Am. Chem. Soc.* **2006**, *128*, 12038.

(91) Hellingwerf, K. J. *Antonie van Leeuwenhoek* **2002**, *81*, 51.

(92) Kort, R.; Vonk, H.; Xu, X.; Hoff, W. D.; Crielaard, W.; Hellingwerf, K. J. *FEBS Lett.* **1996**, *382*, 73.

(93) Hellingwerf, K. J.; Hendriks, J.; Gensch, T. *J. Phys. Chem. A* **2003**, *107*, 1082.

(94) Groenhof, G.; Schafer, L. V.; Boggio-Pasqua, M.; Grubmuller, H.; Robb, M. A. *J. Am. Chem. Soc.* **2008**, *130*, 3250.

(95) Ko, C.; Virshup, A. M.; Martinez, T. J. *Chem. Phys. Lett.* **2008**, *460*, 272.

(96) Gromov, E. V.; Burghardt, I.; Hynes, J. T.; Koppel, H.; Cederbaum, L. S. *J. Photochem. Photobiol., A* **2007**, *190*, 241.

(97) Kim, M.; Hoff, W. D.; Mathies, R. A.; Hellingwerf, K. J. *Biochemistry* **1995**, *34*, 12669.

(98) Lee, I.-R.; Lee, W.; Zewail, A. H. *Proc. Natl. Acad. Sci.* **2006**, *103*, 258.

(99) Ryan, W. L.; Gordon, D. J.; Levy, D. H. *J. Am. Chem. Soc.* **2002**, *124*, 6194.

(100) Espagne, A.; Changenet-Barret, P.; Plaza, P.; Martin, M. M. *J. Phys. Chem. A* **2006**, *110*, 3393.

(101) Changenet-Barret, P.; Plaza, P.; Martin, M. M. *Chem. Phys. Lett.* **2001**, *336*, 439.

(102) Changenet-Barret, P.; Espagne, A.; Katsonis, N.; Charier, S.; Baudin, J.-B.; Jullien, L.; Plaza, P.; Martin, M. M. *Chem. Phys. Lett.* **2002**, *365*, 285.

(103) Larsen, D. S.; Vengris, M.; van Stokkum, I. H. M.; van der Horst, M. A.; Cordfunke, R. A.; Hellingwerf, K. J.; van Grondelle, R. *Chem. Phys. Lett.* **2003**, *369*, 563.

(104) Larsen, D. S.; Vengris, M.; van Stokkum, I. H. M.; van der Horst, M. A.; de Weerd, F. L.; Hellingwerf, K. J.; van Grondelle, R. *Biophys. J.* **2004**, *86*, 2358.

(105) El-Gezawy, H.; Rettig, W.; Danel, A.; Jonusauskas, G. *J. Phys. Chem. B* **2005**, *109*, 18699.

(106) Espagne, A.; Changenet-Barret, P.; Baudin, J.-B.; Plaza, P.; Martin, M. M. *J. Photochem. Photobiol., A* **2007**, *185*, 245.

(107) Espagne, A.; Paik, D. H.; Pascale, C.-B.; Martin, M. M.; Zewail, A. H. *ChemPhysChem* **2006**, *7*, 1717.

(108) Molina, V.; Merchan, M. *Proc. Natl. Acad. Sci.* **2001**, *98*, 4299.

(109) Gromov, E. V.; Burghardt, I.; Koppel, H.; Cederbaum, L. S. *J. Phys. Chem. A* **2005**, *109*, 4623.

(110) Sergi, A.; Gruning, M.; Ferrario, M.; Buda, F. *J. Phys. Chem. B* **2001**, *105*, 4386.

(111) Ko, C.; Levine, B.; Toniolo, A.; Manohar, L.; Olsen, S.; Werner, H.-J.; Martinez, T. J. *J. Am. Chem. Soc.* **2003**, *125*, 12710.

Centennial Feature Article

J. Phys. Chem. B, Vol. 113, No. 11, 2009 **3291**

(112) Li, Q.-S.; Fang, W.-H. *Chem. Phys.* **2005**, *313*, 71.

(113) Yamada, A.; Yamamoto, S.; Yamato, T.; Kakitani, T. *THEOCHEM* **2001**, *536*, 195.

(114) Getzoff, E. D.; Gutwin, K. N.; Genick, U. K. *Nat. Struct. Biol.* **2003**, *10*, 663.

(115) Schoenlein, R. W.; Peteanu, L. A.; Mathies, R. A.; Shank, C. V. *Science* **1991**, *254*, 412.

(116) Ferre, N.; Olivucci, M. *J. Am. Chem. Soc.* **2003**, *125*, 6868.

(117) Yan, E. C. Y.; Kazmi, M. A.; Ganim, Z.; Hou, J. M.; Pan, D. H.; Chang, B. S. W.; Sakmar, T. P.; Mathies, R. A. *Proc. Natl. Acad. Sci.* **2003**, *100*, 9262.

(118) Yan, E. C. Y.; Kazmi, M. A.; De, S.; Chang, B. S. W.; Seibert, C.; Marin, E. P.; Mathies, R. A.; Sakmar, T. P. *Biochemistry* **2002**, *41*, 3620.

(119) Bravaya, K.; Bochenkova, A.; Granovsky, A.; Nemukhin, A. *J. Am. Chem. Soc.* **2007**, *129*, 13035.

(120) Schreiber, M.; Buss, V.; Sugihara, M. *J. Chem. Phys.* **2003**, *119*, 12045.

(121) Okada, T.; Sugihara, M.; Bondar, A.; Elstner, M.; Entel, P.; Buss, V. *J. Mol. Biol.* **2004**, *342*, 571.

(122) Freedman, K.; Becker, R. S. *J. Am. Chem. Soc.* **1986**, *108*, 1245.

(123) Nielsen, I. B.; Lammich, L.; Anderson, L. H. *Phys. Rev. Lett.* **2006**, *96*, 018304.

(124) Shichida, Y.; Matuoka, S.; Yoshizawa, T. *Photobiochem. Photobiophys.* **1984**, *7*, 221.

(125) Ben-Nun, M.; Martinez, T. J. *Chem. Phys. Lett.* **1998**, *290*, 289.